Geophysical Research Letters

RESEARCH LETTER
10.1029/2018GL081806

The Two Diurnal Modes of Tropical Upward Motion

James H. Ruppert Jr.[1,2] **and Daniel Klocke**[3]

[1]Max Planck Institute for Meteorology, Hamburg, Germany, [2]Now at the Department of Meteorology and Atmospheric Science, The Pennsylvania State University, University Park, PA, USA, [3]Hans Ertel Center for Weather Research, Deutscher Wetterdienst, Offenbach, Germany

Key Points:
- Tropical upward motion exhibits a bimodal diurnal cycle with a top-heavy shape during the day and a bottom-heavy shape at night
- The diurnal radiative heating cycle within anvil clouds is critical to upper-level diurnal circulation change
- Upper-level lifting due to daytime cloud-shortwave heating causes an afternoon peak in anvil clouds, indicating a feedback

Supporting Information:
- Supporting Information S1
- Figure S1

Correspondence to:
J. H. Ruppert Jr.,
james.ruppert@psu.edu

Citation:
Ruppert, J. H., Jr, & Klocke, D. (2019). The two diurnal modes of tropical upward motion. *Geophysical Research Letters*, *46*, 2911–2921. https://doi.org/10.1029/2018GL081806

Received 21 DEC 2018
Accepted 25 FEB 2019
Accepted article online 4 MAR 2019
Published online 9 MAR 2019

Abstract This study describes a new mechanism governing the diurnal variation of vertical motion in tropical oceanic heavy rainfall zones, such as the intertropical convergence zone. In such regions, the diurnal heating of widespread anvil clouds due to shortwave radiative absorption enhances upward motion in these upper layers in the afternoon. This radiatively driven ascent promotes an afternoon maximum of anvil clouds, indicating a diurnal cloud-radiative feedback. The opposite occurs at nighttime: While rainfall exhibits a dominant peak at night-early morning, the boundary layer rooted upward motion and latent heating tied to this peak are forced to be more bottom heavy by the nighttime anomalous radiative cooling at upper levels. This mechanism therefore favors the stratiform top-heavy heating mode during daytime and suppresses it nocturnally. These diurnal circulation signatures arise from microphysical-radiative feedbacks that manifest on the scales of organized deep convection, which may ultimately impact the daily mean radiation budget.

Plain Language Summary Observations show that the rainfall in tropical thunderstorms over the oceans peaks at night-early morning. This is because solar radiation leads to warming in the upper troposphere in rainy and cloudy regions, which suppresses the convective overturning motions that cause the rainfall. Given the nocturnal peak in rainfall, we intuitively expect the upper-level outward spreading anvil clouds of thunderstorms to maximize at night, when thunderstorms are strongest. While anvil clouds indeed peak at night, they additionally peak in the midafternoon, which cannot be explained by this nocturnal convection. In this study we show through global model simulations that the afternoon peak of anvil clouds over tropical oceans is caused by the upper-cloud daytime maximum of radiative warming. Although this radiative warming suppresses convective motions (and hence rainfall), it causes a circulation response in the upper troposphere that manifests in locally increased upward motion. This upward motion enhances the production and spreading of anvil clouds in the afternoon.

1. Introduction

Tropical rainfall variability is dominated by the diurnal cycle, which manifests both over land and sea (Chen & Houze, 1997; Dai, 2001; Gray & Jacobson, 1977; Kikuchi & Wang, 2008; Ruppert & Johnson, 2015). The character of the diurnal cycle is sensitive to the underlying surface type and its heterogeneity (Johnson, 2011; Yang & Smith, 2006). Over the open ocean, radiative heating and its interaction with clouds plays a dominant role in diurnally modulating deep convection, causing rainfall to peak at night-early morning (Gray & Jacobson, 1977; Kraus, 1963; Randall et al., 1991). Fully understanding the interaction between radiative heating, circulation, and clouds on this time scale is a challenge, since the transient impacts of gravity waves can regularly manifest within it (Nicholls, 2015; O'Neill et al., 2017; Ruppert & Hohenegger, 2018). Yet understanding this interplay is critical to both resolving deficiencies of the diurnal cycle in climate models (Dirmeyer et al., 2012; Jiang et al., 2015) and understanding how it impacts the radiation budget at longer time scales (Bergman & Salby, 1997; Cronin et al., 2015; Ruppert, 2016). This study investigates the diurnal interaction between clouds, circulation, and radiative heating in the context of the intertropical convergence zone (ITCZ), the ascending branch of the Hadley cell.

Over the tropical oceans, the majority of rainfall is explained by extensive and often long-lived clusters of deep convection, which prevail in the monsoon trough, the ITCZ, and favorable regions of equatorial waves (Chen & Houze, 1997; Gray & Jacobson, 1977; Mapes & Houze, 1993; Nesbitt & Zipser, 2003; Wheeler & Kiladis, 1999). The extensive, optically opaque anvil clouds that characterize these organized clusters are

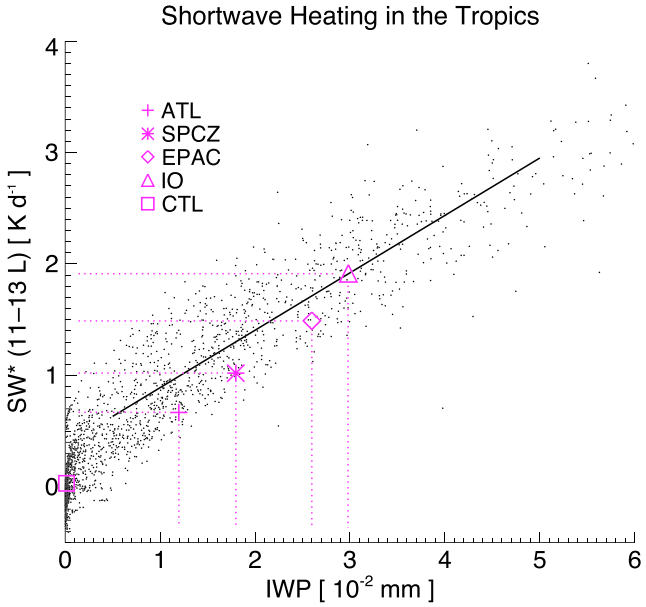

Figure 1. Differential shortwave heating (SW*; from 11–13 local time (L); K/day) estimated from a model (described in section 2), versus daily mean IWP (10^{-2} mm; = 10 g/m^2). SW* is calculated as the total heating with the cloud-free profile subtracted; averaged from 9–14 km vertically; for ocean points from 15°S to 15°N binned 2 × 2° spatially; and from output temporally averaged from 19–39 days. The cloud-free profile is the average of columns where IWP ≤ 10^{-3} mm. The linear fit (0.52 K day per 10^{-2} mm) is calculated for 0.5 ≤ IWP ≤ 5×10^{-2} mm. ATL = Atlantic; CTL = control; EPAC = East Pacific; IO = Indian Ocean; IWP = ice water path; SPCZ = South Pacific Convergence Zone.

especially important to the diurnal cycle, where the high concentration of hydrometeors and elevated water vapor strongly interact with radiative fluxes compared to their dry, cloud-free surroundings (Webster & Stephens, 1980). The footprint of these clouds in longwave heating (LW*) manifests in enhanced cooling from cloud top, with heating within and below their bases due to the local greenhouse effect of both clouds and water vapor (Albrecht & Cox, 1975). The radiative signature of these clouds in shortwave heating (SW*) is essentially the opposite: Direct shortwave absorption causes strong upper-cloud heating, while cloud shading greatly suppresses heating in the lower troposphere (Cox & Griffith, 1979; Webster & Stephens, 1980). It is of course the diurnal variation of SW* that causes the diurnal cycle in convection.

While it is widely appreciated that high clouds reflect shortwave flux out to space, their impact in directly heating the upper troposphere through shortwave absorption, especially in the near infrared, is likely much less appreciated (Ackerman et al., 1988). This absorption increases in proportion with optical depth, resulting in heating rates that often exceed 30 K/day during midday hours in the vicinity of strong convection (Ackerman et al., 1988; Powell et al., 2012; Webster & Stephens, 1980). The large-scale signature of this effect is demonstrated in Figure 1, where large-scale-binned SW* is plotted as a function of ice water path (IWP), as estimated from a model (described in section 2). The relationship between SW* and IWP is remarkably linear, with SW* increasing by 0.52 K/day per 10^{-2} mm of IWP for ~ 0.5 ≤ IWP ≤ 5 × 10^{-2} mm. The magenta markers exemplify climatological zones of deep convection and a control region (CTL) of mean subsidence (discussed later).

On one hand, the diurnal cycle of SW* increases the static stability in cloudy regions during daytime and decreases it at night, which is argued to be the primary cause for the nocturnal-early-morning peak in rainfall over tropical oceans (Liu & Moncrieff, 1998; Randall et al., 1991; Ruppert & Hohenegger, 2018). On the other hand, the dramatic diurnal reversal of upper-level heating due to SW* may directly modulate upper-level circulation (Figure 1), especially given that this heating is localized to anvil clouds, with quasi-steady cooling in their clear-air surroundings (Cox & Griffith, 1979; Dai & Deser, 1999; Gray & Jacobson, 1977; Ruppert & Hohenegger, 2018). This effect may indeed manifest in the ITCZ and Hadley cell (Ackerman et al., 1988; Ciesielski et al., 2018; Webster & Stephens, 1980). While variations in latent heating are undoubtedly much larger in magnitude than those of radiative heating in the low-middle-troposphere, this is not strictly the

case in the upper-cloud region where SW* maximizes (Ciesielski et al., 2017; Johnson et al., 2015; Johnson et al., 2016; Schumacher et al., 2007).

Two hypotheses are examined in this study in light of the large relative magnitude of SW* in the upper troposphere of convective regions. First, (H1) *shortwave-anvil cloud heating causes a daytime increase in upward motion in the tropical upper troposphere.* This hypothesis is supported by recent in situ observations of circulation in the ITCZ and Hadley cell of the Indian Ocean (IO; Ciesielski et al., 2018) and idealized simulations conducted in the diurnal radiative-convective equilibrium framework (Ruppert & Hohenegger, 2018). Second, satellite retrievals reveal an afternoon peak in both upper-tropospheric water vapor and optically thick clouds (Gupta et al., 2018; Jiang et al., 2015; Soden, 2000; Wu & Ruan, 2016). We therefore hypothesize that (H2) *The shortwave radiatively driven increase of upper-level lifting during daytime causes a daytime peak in upper-level cloud amount.* We examine these two hypotheses here in the context of the ITCZ and coupled circulation through a global storm-resolving numerical model framework.

2. Study Methods

A global storm-resolving model simulation is performed with the icosahedral nonhydrostatic (ICON) model, using a framework similar to that of Klocke et al. (2017). ICON is a unified system for both numerical weather prediction (Zängl et al., 2015) and research (Crueger et al., 2018; Giorgetta et al., 2018), developed jointly by the German weather service (Deutscher Wetterdienst) and Max Planck Institute for Meteorology. The framework employed herein invokes surface and atmospheric physics parameterizations designed for and tested at storm-resolving scales (Klocke et al., 2017).

A global model grid is employed at the gray zone, in that individual convective cloud elements are underresolved, while mesoscale convective systems and their upscale link with circulation are resolved. The grid is formulated as a Delauney mesh of triangular cells, with the square root of the mean cell area equal to 5 km. A generalized height-based vertical (z) coordinate of 90 levels is employed. Over oceans, this grid can be described as follows: $\Delta z = 20$ m just above the surface, $\Delta z = 400$ m for $6 \leq z \leq 14$ km, with Δz stretching thereafter to a maximum of ~2.6 km at the model top (75 km). A sponge layer spans from 44 km to model top to absorb gravity waves. The dynamical core employs Arakawa C-grid staggering (Zängl et al., 2015). Several physics parameterizations developed for numerical weather prediction applications are invoked (Baldauf et al., 2011), including a turbulent kinetic energy framework for subgrid-scale turbulence; a single-moment microphysics scheme that predicts cloud water, rainwater, cloud ice, snow, and graupel; and an interactive surface flux scheme. Interactive radiation is calculated every 15 min using the RRTM-G scheme (Clough et al., 2005; Iacono et al., 2008; Mlawer et al., 1997).

The initial conditions are prescribed using the atmospheric analysis for 1 August 2016 from the European Centre for Medium-Range Weather Forecasts analysis taken from a 9.5-km grid. The simulation is freely run from this state for 40 days. Sea surface temperature (SST) is fixed to this initial state, with no skin temperature parameterization. This simulation therefore presents a unique opportunity to assess the distinct role of direct cloud-radiation interaction in the diurnal cycle, absent the diurnal variation of SST, which is known to modulate convection in suppressed regimes (Ruppert & Johnson, 2015, 2016; Ruppert, 2016; Sui et al., 1997; Webster et al., 1996). A global animation of the entire simulation can be found at YouTube (https://www.youtube.com/watch?v=XEB4tGXiJzU).

For all analysis, model output is regridded to a 0.5° latitude-longitude grid. This regridding averages over many individual convective elements, thus retaining only their coupling with larger-scale circulation. Analysis is conducted from hourly output. Radiative tendencies were only output at 3-hourly frequency and thus are linearly interpolated to hourly for analysis purposes. All output is translated to local time (L).

To characterize the mean conditions and diurnal cycle of deep convection over the open ocean and assess sensitivities to regional differences, a set of composites are generated over 19–39 days of the simulation. The tropics are in approximate radiative-convective equilibrium by this time. Composites are generated for the four regions demarcated by solid boxes in Figure 2b (modest changes in the boundaries had negligible effect). These regions are denoted East Pacific (EPAC), Atlantic (ATL), IO, and the South Pacific Convergence Zone (SPCZ). The region outlined by the dashed box (CTL) is characterized by suppressed deep convection, more closely resembling a trade cumulus regime, and thereby serves as a control for the study. For the four deep convection composites, longitudinal bounds are first selected to identify areas of interest. The latitudinal

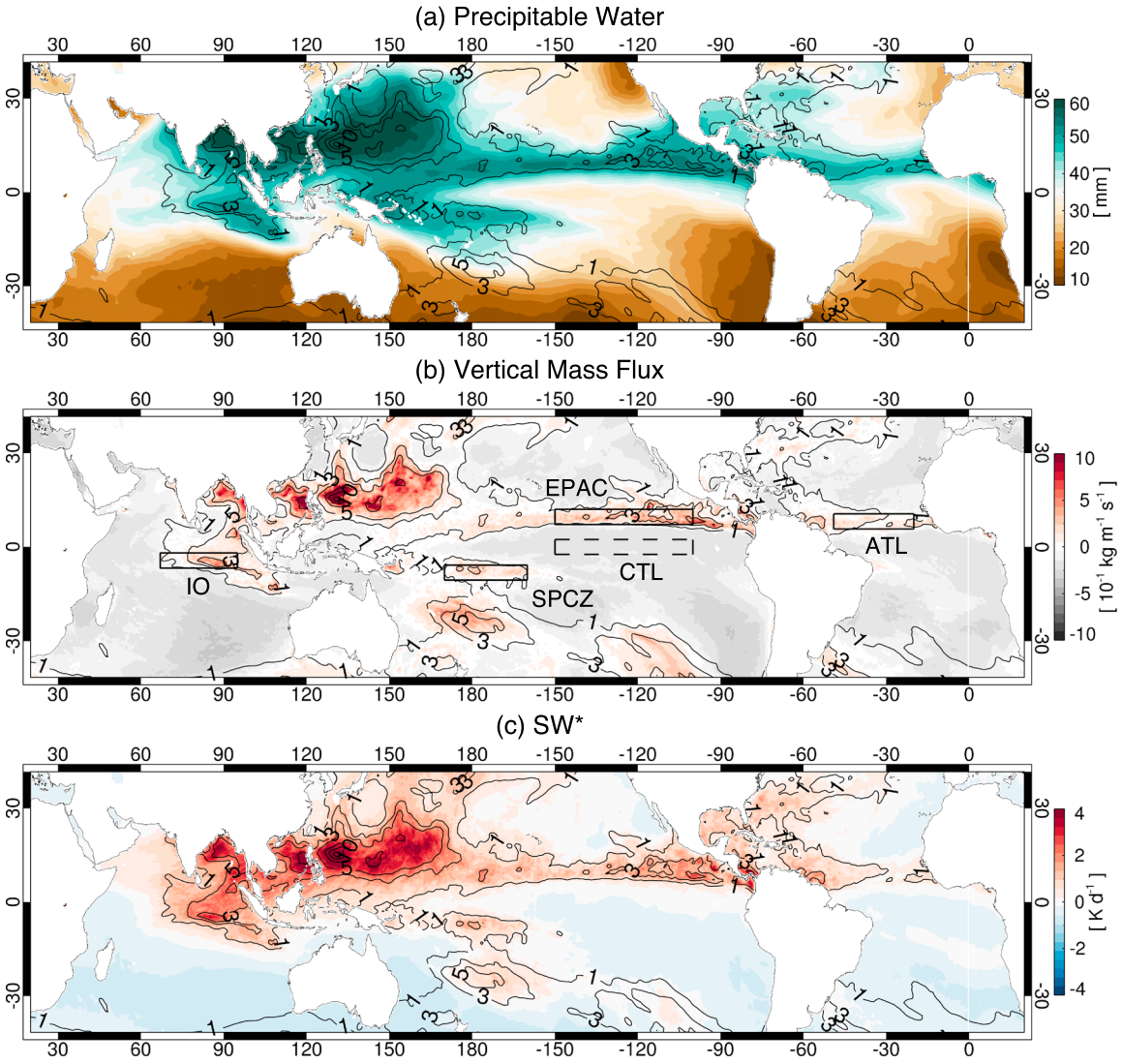

Figure 2. Time mean maps from 19–39 days, with (a) precipitable water (shading; mm), (b) column-integrated vertical mass flux (shading; 10^{-1} kg·m^{-1} ·s^{-1}), and (c) SW* (shading; 10^{-1} K/day) averaged over 9–14 km and from 11–13 L. ice water path is contoured at 1, 3, 5, 10, and 15×10^{-2} mm. The boxes in (b) indicate selected composite regions. ATL = Atlantic; CTL = control; EPAC = East Pacific; IO = Indian Ocean; SPCZ = South Pacific Convergence Zone.

bounds are then objectively identified as a 5° north-south swath centered on the latitude of maximum vertically integrated vertical mass flux (Figure 2b). Results are qualitatively insensitive to the width of this latitudinal swath. The CTL region is simply the EPAC region shifted 10° southward.

3. Results

The global distribution of deep convection in the model simulation is characterized through time mean precipitable water (PW), column-integrated vertical mass flux, and IWP in Figures 2a and 2b. Climatological zones of deep convection are identifiable as local maxima in each quantity, which exhibit a preference for the Northern Hemisphere owing to the August SST and solar heating state. The deep convection composite zones (solid boxes) bare resemblance to observed climatological features, with what will be referred to as ITCZs in the EPAC, ATL, and IOs, and the SPCZ. The northwest Pacific is characterized by the strongest deep convection, owing to tropical cyclones that tended to form over anomalously warm SST (not shown). This study focuses on the more linear zones selected for compositing, which sample a range in mean strength of convective activity.

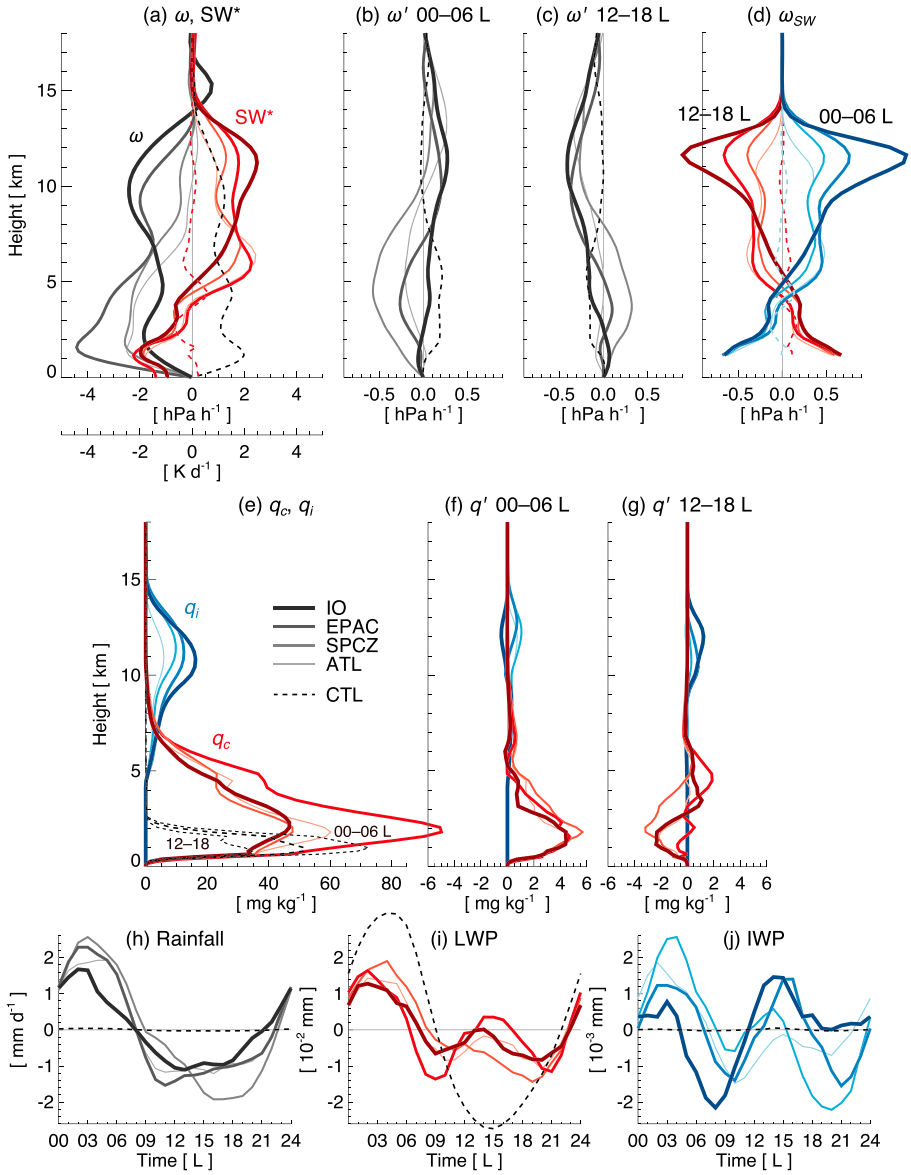

Figure 3. Composites for the selected regions marked by rectangles in Figure 2b, with line thickness and color pigment proportional to magnitude of IWP (or SW*; Figure 1). (a) Mean vertical pressure velocity ω (gray-black; hPa/hr) and SW* averaged from 11–13 L (reds; K/day), and ω' (deviation from daily mean) averaged over (b) 00–06 and (c) 12–18 L. (d) As in (b) and (c) except for the diagnostic motion due to SW ω_{SW}. (e–g) As in (a)–(c) except with cloud liquid water (q_c; red) and cloud ice (q_i; blue; mg/kg). Profiles of q_c and q_i (=0) for CTL are only included in panel (d), with the daily mean (thick dashed) and means for 00–06 and 12–18 L (thin dashed) as labeled. Lastly, time series of (h) rainfall (mm/hr), (i) liquid water path (LWP; 10^{-2} mm), and (j) IWP (10^{-3} mm = g/m^2) with time means subtracted. ATL = Atlantic; CTL = control; EPAC = East Pacific; IO = Indian Ocean; IWP = ice water path; LWP = liquid water path; SPCZ = South Pacific Convergence Zone.

The four deep convection composite regions are roughly east-west oriented convergence zones, characterized by local maxima in PW (>45 mm) and mean upward motion. IWP also peaks in these regions ($\geq 1 \times 10^{-2}$ mm) owing to a high frequency of anvil clouds. Given abundant anvils and high IWP, SW* is elevated in these regions (Figure 2c). Upper-level SW* is negligible in the regions bordering the convective zones, where anvils and advected ice occur less frequently and is weakly negative farther from these zones where ice clouds are exceedingly scarce. CTL is one such region, situated south of EPAC in an area of subsidence. Mean values of IWP and SW* for each region are shown in Figure 1, which fall roughly in line with the linear fit between SW* and IWP. Values in both measures increase in the following order: CTL,

ATL, SPCZ, EPAC, and IO. IO is characterized by the maximum values, which are 3×10^{-2} mm in IWP and 1.9 K/day in SW*, while CTL is characterized by approximately zero in both quantities.

Time mean profiles of vertical pressure velocity ω, SW*, and specific cloud q_c and ice q_i water content are provided in Figures 3a and 3e, composited by region. Each of the convective regions is characterized by upward motion, with its magnitude in the upper troposphere (above 7 km) varying in proportion with IWP and SW* (Figure 3a). Upper-level upward motion is weakest in ATL, greater in SPCZ, and so forth. Both EPAC and IO are characterized by notable upper-level peaks, with $\omega \leq -2$ hPa/hr, which are at ~9 km in EPAC and 10 km in IO. These upper-level peaks coincide with enhanced midlevel convergence, which in turn indicates that the convective systems in these regions contain a large proportion of stratiform precipitation (Houze, 1997; Mapes & Houze, 1995; Zipser, 1977). Mean q_i-amount scales in proportion with "top heavyness" in ω (Figure 3e), and therefore, so too does IWP (Figure 1).

Among the deep convective regions, mean q_c varies in rough proportion with upward motion in the lower troposphere. EPAC exhibits particularly large low-level peaks in both quantities (between 1.5 and 2 km), indicating particularly strong boundary layer convergence. This likely owes to the strong meridional SST gradient in this region (Back & Bretherton, 2009). CTL exhibits mean subsidence throughout the column and a peak in q_c of ~50 mg/kg near 1 km in height. This peak in low-level cloud in association with mean subsidence and suppressed ice is consistent with a trade cumulus regime (Nitta & Esbensen, 1974).

The proportional relationship between SW* in the upper troposphere and q_i (Figure 3a) attests to the role of shortwave-ice cloud heating (Figures 1 and 2c). IO exhibits the greatest magnitude of SW* heating, which peaks (2.5 K/day) at ~11.5 km vertically. The peaks in SW* from ~6–7 km in EPAC, SPCZ, and ATL likely owe to SW absorption by midlevel clouds and humidity layers. The negative values of SW* in the lower troposphere in the deep convective regions owes to elevated SW heating at these levels outside of the convective areas, where a lack of middle- and upper-level clouds allows for greater downwelling shortwave flux. The combination of these two effects results in a very top-heavy profile of SW* in the convective regions (Ruppert & Hohenegger, 2018). The SW* profile for CTL, in contrast, is close to 0 through most of the column, since it is close to the subtracted ice-free profile. This top-heavy SW* profile in the deep convective areas causes a pronounced diurnal variation in the vertical shape of total radiative heating in these regions. This change causes tropospheric static stability to increase in convective regions during daytime and decrease during nighttime, which explains the nocturnal invigoration of convection and rainfall to first order (Liu & Moncrieff, 1998; Randall et al., 1991; Ruppert & Hohenegger, 2018). The low-level diurnal radiation-circulation adjustment mechanism of Gray and Jacobson (1977) augments this nocturnal peak (Nicholls, 2015; Ruppert & Hohenegger, 2018). Latent heating from this nocturnally enhanced convection increases upward motion in the lower-midtroposphere (Ruppert & Hohenegger, 2018). This effect is shown in ω', the deviation of ω from its daily mean, from 00–06 L (Figure 3b).

The nocturnal increase of rainfall in the deep convective regions is depicted through composite diurnal time series with the mean subtracted (Figure 3h). Rainfall peaks between 02 and 05 L, roughly consistent with observations (Kikuchi & Wang, 2008), with broader minima between ~10 and 21 L. The mean amplitude of this variation is 1.8 mm/day or 16% of the mean rainfall rate (11.1 mm/day). Cloud liquid water path (LWP; i.e., the column integration of q_c) exhibits a bimodal diurnal cycle, with one peak closely coinciding with rainfall and a secondary peak in the afternoon between 12 and 17 L (Figure 3i). The diurnal cycle of IWP exhibits an afternoon peak of the same timing that is much more prominent relative to that in LWP (Figure 3j). The magnitude of this afternoon peak in IWP relative to the nocturnal peak increases in proportion to time mean IWP among the composite regions (Figure 1); that is, it is largest in IO, smaller in EPAC, and so forth. The amplitude of these diurnal variations in LWP and IWP is approximately 1.2×10^{-2} mm (6% of the mean) and 1.5×10^{-3} mm (7%), respectively. What causes this afternoon peak in IWP, considering that deep convection is diurnally suppressed at this time? Diurnal circulation changes shed light on this question.

The diurnal change in ω in the composite regions is shown in Figures 3b and 3c. Most of the convective regions are characterized by anomalous rising motion in the lower-midtroposphere and subsidence in the upper troposphere in the 00–06 L profiles, with roughly the opposite vertical structure in the 12–18 L profiles. This circulation change implies a diurnal variation of the vertical mass pumping of the Hadley cell. The magnitude change of ω is ~0.5 hPa/hr in the convective regions, which is approximately 25% of the mean magnitude of ω (Figure 3a). In situ observations from a field campaign in the IO demonstrate a very similarly

patterned diurnal change in ω in the ITCZ, yet with a remarkable composite mean diurnal range of between 60% and 80% relative to the time mean (Ciesielski et al., 2018). Further study is required to pin down the climatological magnitude of this range. We move forward, nevertheless, given this evidence that the model adequately represents diurnal changes in circulation linked to convection.

While the nocturnal increase of latent heating (Figure 3h) linked to boundary layer rooted convection is likely critical to the diurnal change in ω in the lower-midtroposphere (Ciesielski et al., 2018; Ruppert & Hohenegger, 2018), here we test the notion that SW* directly drives the circulation change in the middle-upper troposphere. This effect can be approximated from the weak temperature gradient approximation (Sobel et al., 2001) through

$$\omega_{SW} = [SW^*]' \left(\frac{\partial s}{\partial p} \right)^{-1}, \tag{1}$$

where s is dry static energy, and $[\ ]'$ denotes a deviation from the daily mean (Ruppert & Hohenegger, 2018; Schulz & Stevens, 2018). ω_{SW} is shown in Figure 3d for night and day. ω_{SW} exhibits a pronounced top-heavy pattern of upper-level rising motion during daytime, with essentially the opposite sign of this pattern at night (longwave heating has negligible diurnal change; not shown). The profiles of ω_{SW} and ω' approximately match in magnitude in the middle-upper troposphere, although ω_{SW} (especially in IO) contains some higher-order modes that do not appear in ω' (the influence of each mode on ω scales with its depth; Herman & Raymond, 2014; Ruppert & Hohenegger, 2018).

Thus, the actual diurnal circulation change in the middle-upper troposphere can be explained by the day-night reversal from top-heavy heating to cooling due to SW*: While enhanced daytime upper-level lifting is caused by daytime shortwave heating, anomalous nocturnal radiative cooling promotes anomalous downward motion. A sensitivity experiment in which ice clouds are made radiatively inactive supports the argument that ice-shortwave interaction is especially important to this diurnal circulation change in heavily ice-laden zones of deep convection (supporting information Figure S1). Given the influence of ω over latent heating, this circulation response to shortwave heating likely suppresses the stratiform top-heavy latent heating mode nocturnally and supports it during daylight hours (Ciesielski et al., 2018).

The afternoon peak in upward motion at upper levels driven by SW* explains the afternoon peak in IWP, which is 2–4 hr after peak solar heating (12 L; Figure 3j). This afternoon peak in ice indicates a feedback from SW* and supports the notion that ω_{SW} promotes stratiform (upper-level) latent heating during daytime. The daytime increase in upper-level upward motion also likely explains the secondary afternoon peak in LWP (Figure 3i). Profiles of q_c and q_i with the daily mean removed (q_c' and q_i') depict the vertical structure of these diurnal changes in cloud water (Figures 3f and 3g). The afternoon peaks in q_i' (daily mean removed) are vertically centered between ~10.5 and 12 km (Figure 3g). The nocturnal-early-morning peaks in q_i' are generally higher, suggesting that nocturnally invigorated convection penetrates deeply and detrains at a higher level than the anvil clouds produced by the circulation response to shortwave-cloud heating. q_c' is primarily positive in the profiles for night-early morning (Figure 3f). In the afternoon profiles, it is positive only above ~3 km in EPAC and IO and is otherwise negative. In IO, ω' exhibits anomalous upward motion in the afternoon reaching down to 3 km, although in EPAC it only reaches 5.5 km. We therefore speculate that positive afternoon q_c' from 3–5 km at least partly owes to falling ice and/or lingering cloud from earlier convection.

A diurnal time height series of ω and q_i' for EPAC reaffirms that the afternoon peak in q_i' is slightly lower vertically (by ~2.5 km) than the nocturnal peak (Figure 4a). The higher nocturnal peak linked to nocturnal deep convection coincides with peaks in rainfall, IWP, and LWP. The lower afternoon peak coincides with diurnally suppressed rainfall and owes to the afternoon increase of upper-level upward motion, as described above. Meridional cross sections for 00–06 and 12–18 L indicate that the nocturnal peak in q_i' is more latitudinally confined, with the greatest magnitude in a ~2.5° latitude span (Figure 4b). The afternoon peak, however, is manifest in dual peaks, which together span nearly 8° of latitude, stretching beyond the bounds of the EPAC composite region (Figure 4c). In the afternoon, upward motion peaks vertically at 9–10 km, indicating enhanced divergence in the layer ~10–12 km through mass continuity (Figures 4a and 4c). This more latitudinally dispersive afternoon pattern in q_i' can therefore be explained as a consequence of enhanced upper-tropospheric divergent outflow.

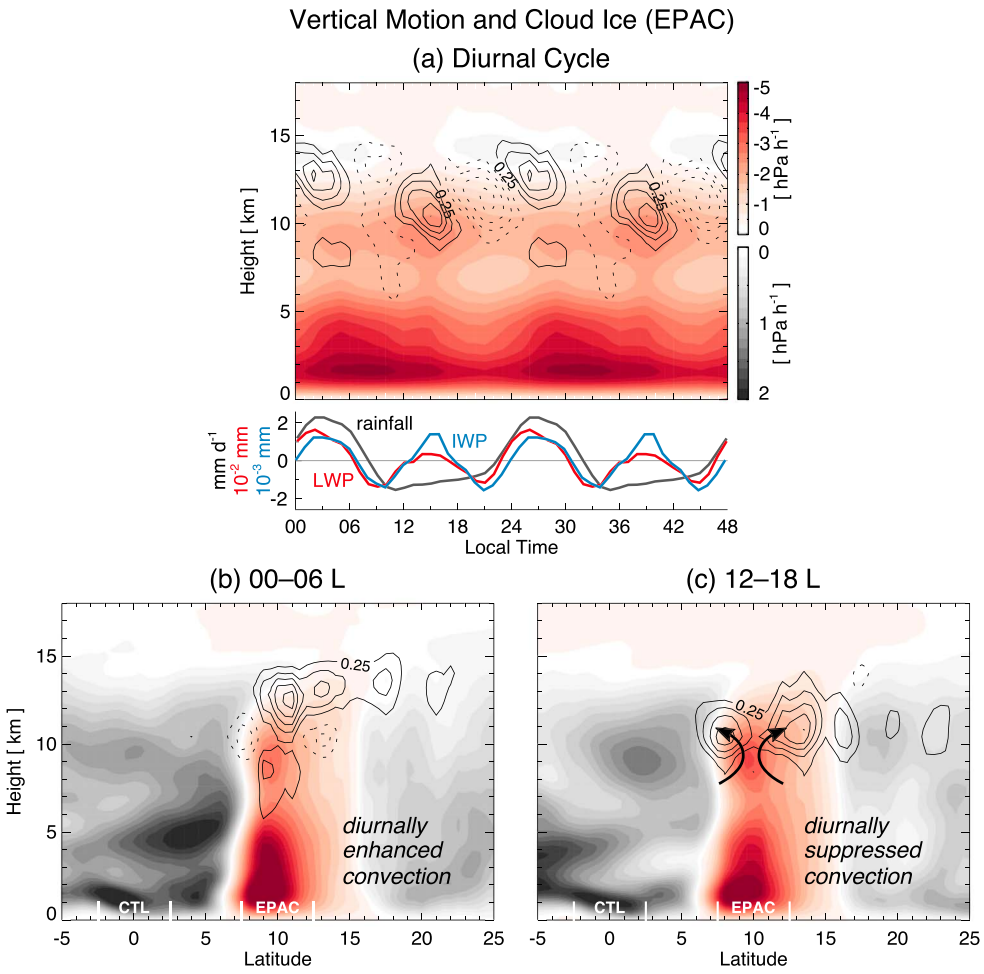

Figure 4. (a) Composite mean diurnal time series for EPAC of (upper) ω (shading; hPa/hr) and q_i' (contours every 0.25 mg/kg; negative dashed, zero-contour omitted) and (lower) rainfall, LWP, and IWP with means removed, repeated for continuity. (b, c) Meridional cross sections zonally averaged across EPAC and CTL averaged over (b) 00–06 and (c) 12–18 L. The latitude bands of EPAC and CTL are indicated along the abscissa. CTL = control; EPAC = East Pacific; IWP = ice water path; LWP = liquid water path.

The CTL region features no ice and hence near-zero SW* (Figures 1 and 3a). In line with the argument that the diurnal cycle of SW* is critical to the diurnal variation of circulation at upper levels, CTL is not characterized by an afternoon increase in upward motion in the upper troposphere (Figure 3c). Enhanced subsidence is apparent between 1 and 9 km in the profile for 00–06 L (Figure 3b). The meridional cross sections indicate that subsidence is enhanced both north and south of the ITCZ at this time in comparison to 12–18 L (Figures 4b and 4c). In the cross section for 12–18 L, subsidence is weaker flanking the ITCZ from the surface to ~8 km, although localized maxima in subsidence appear from ~8–12 km. This is consistent with in situ observations of the Hadley cell described by Ciesielski et al. (2018). Gonzalez et al. (2017) showed through theoretical arguments that transient heating in an ITCZ situated north of the equator will cause stronger compensating subsidence and inertia-gravity wave activity on its southern side. The subsidence flanking the ITCZ in these cross sections is indeed stronger to the south, consistent with that finding (Figures 4b and 4c). We therefore speculate that the low-midlevel and upper-level diurnal maxima in subsidence flanking the ITCZ are the transient response to nocturnal latent heating and daytime shortwave heating, respectively (Gonzalez et al., 2017). More work is required, however, to investigate this transient, remote response.

While CTL is characterized by negligible mean rainfall (0.05 mm/day), and hence a negligible diurnal cycle of rainfall, LWP exhibits a notable diurnal variation with amplitude approximately 3.0 $\times 10^{-2}$ mm (45% of the mean) and a nocturnal peak at ~4 L. This variation is consistent in timing with satellite retrievals described by Wood et al. (2002), although the simulated amplitude is on the upper end of those observations.

Subsidence is enhanced at the time of peak LWP in CTL (Figure 3b), suggesting that subsidence drying has very little effect on these clouds compared to the nocturnal increase of radiative cooling from these clouds (Caldwell & Bretherton, 2009).

4. Summary and Conclusions

In this study we have demonstrated through global storm-resolving numerical modeling that the upward motion in the ITCZ—the ascending branch of the Hadley cell—is characterized by a pronounced, bimodal diurnal cycle, due to the out-of-phase forcing from low- to middle-level latent heating and upper-level shortwave heating. The optically opaque anvil clouds that characterize the ITCZ, that is, the vigorous deep convective systems within it, are strongly heated during daylight hours by shortwave flux absorption. While the influence of this top-heavy heating on static stability nocturnally promotes boundary layer rooted convection and rainfall, it additionally drives a thermally direct circulation response at upper levels, manifest in enhanced lifting during daytime and downward motion at night. This diurnal circulation adjustment therefore favors the stratiform (top-heavy) latent heating mode during daytime and suppresses it at night, thus favoring bottom-heavy nocturnal convection. The daytime radiatively induced upper-level lifting promotes an afternoon peak in anvil clouds of similar and sometimes greater magnitude to the nocturnal peak, indicative of a diurnal cloud-radiative feedback.

This effect has been drawn out herein from large-scale averages composited over many days. On these scales, the effect of shortwave absorption by anvil clouds is exemplified by the linear increase of upper-level shortwave heating with IWP (Figure 1). Yet on the scales of individual convective cloud clusters, shortwave heating rates readily exceed 30 K/day (Ackerman et al., 1988; Powell et al., 2012; Webster & Stephens, 1980). This implies that the effects of diurnal circulation adjustment described above are amplified on these scales.

Two hypotheses were presented in section 1: (H1) *Shortwave-anvil cloud heating causes a daytime increase in upward motion in the tropical upper troposphere* and (H2) *The shortwave radiatively driven increase of upper-level lifting during daytime causes a daytime peak in upper-level cloud amount.* The findings of this study support both of these hypotheses and emphasize that the upward motion in organized tropical deep convective systems is characterized by a bimodal diurnal cycle upward motion peaks nocturnally in the lower-midtroposphere and peaks in the afternoon in the upper troposphere. Such an evolution manifests in the ITCZ (Ciesielski et al., 2018), mesoscale convective clusters (Ruppert & Hohenegger, 2018), and tropical cyclones (Navarro & Hakim, 2016; Ruppert & O'Neill, 2019).

These findings attest to the sensitivity of tropical circulation at upper levels to diurnally varying cloud-radiative heating, given the relative weakness of latent heating and large magnitude of radiative heating at these levels. These findings additionally emphasize the importance of properly representing diurnal microphysical-radiative feedbacks on the primary scales of organized deep convection, of O(10 km). Failure to do so may bias the daily mean radiation budget, which could translate to large-amplitude biases at longer time scales. Further study is critical to examine this potential time scale feedback.

Acknowledgments
J. H. R. acknowledges funding for this research from the National Science Foundation (Grant AGS-1524844) and Alexander von Humboldt Foundation/Stiftung. D. K. acknowledges funding through the Hans Ertel Center for Weather Research (HErZ). This German research network of universities, research institutions, and DWD is funded by the BMVI (Federal Ministry of Transport and Digital Infrastructure). We thank Claudia Stephan and three anonymous reviewers for their highly constructive comments, Felicia Brisc of Climate Visualization Laboratory (Center for Earth System Research and Sustainability) for creating and sharing the online animation, and the DWD and the Deutsches Klimarechenzentrum (DKRZ) for providing vital supercomputing resources. All model source code, start data, and postprocessing software used in this study are available online; to ensure reproducibility, representative model output and documentation of the model and software versions employed herein can be obtained with no restrictions from the Max Planck Society at the website (https://pure.mpg.de/pubman/faces/HomePage.jsp).

References

Ackerman, T. P., Liou, K.-N., Valero, F. P. J., & Pfister, L. (1988). Heating rates in tropical anvils. *Journal of the Atmospheric Sciences*, *45*(10), 1606–1623. https://doi.org/10.1175/1520-0469(1988)045<1606:HRITA>2.0.CO;2

Albrecht, B., & Cox, S. K. (1975). The large-scale response of the tropical atmosphere to cloud-modulated infrared heating. *Journal of the Atmospheric Sciences*, *32*(1), 16–24. https://doi.org/10.1175/1520-0469(1975)032<0016:TLSROT>2.0.CO;2

Back, L. E., & Bretherton, C. S. (2009). On the relationship between SST gradients, boundary layer winds, and convergence over the tropical oceans. *Journal of Climate*, *22*(15), 4182–4196. https://doi.org/10.1175/2009JCLI2392.1

Baldauf, M., Seifert, A., Förstner, J., Majewski, D., Raschendorfer, M., & Reinhardt, T. (2011). Operational convective-scale numerical weather prediction with the COSMO model: Description and sensitivities. *Monthly Weather Review*, *139*(12), 3887–3905. https://doi.org/10.1175/MWR-D-10-05013.1

Bergman, J. W., & Salby, M. L. (1997). The role of cloud diurnal variations in the time-mean energy budget. *Journal of Climate*, *10*(5), 1114–1124. https://doi.org/10.1175/1520-0442(1997)010<1114:TROCDV>2.0.CO;2

Caldwell, P., & Bretherton, C. S. (2009). Large eddy simulation of the diurnal cycle in Southeast Pacific stratocumulus. *Journal of the Atmospheric Sciences*, *66*(2), 432–449. https://doi.org/10.1175/2008JAS2785.1

Chen, S. S., & Houze, R. A. (1997). Diurnal variation and life-cycle of deep convective systems over the tropical Pacific warm pool. *Quarterly Journal of the Royal Meteorological Society*, *123*(538), 357–388. https://doi.org/10.1002/qj.49712353806

Ciesielski, P. E., Johnson, R. H., Jiang, X., Zhang, Y., & Xie, S. (2017). Relationships between radiation, clouds, and convection during DYNAMO. *Journal of Geophysical Research: Atmospheres*, *122*, 2529–2548. https://doi.org/10.1002/2016JD025965

Ciesielski, P. E., Johnson, R. H., Schubert, W. H., & Ruppert, J. H. (2018). Diurnal cycle of the ITCZ in DYNAMO. *Journal of Climate*, *31*(11), 4543–4562. https://doi.org/10.1175/JCLI-D-17-0670.1

Clough, S. A., Shephard, M. W., Mlawer, E. J., Delamere, J. S., Iacono, M. J., Cady-Pereira, K., et al. (2005). Atmospheric radiative transfer modeling: A summary of the AER codes. *Journal of Quantitative Spectroscopy and Radiative Transfer*, *91*(2), 233–244. https://doi.org/10.1016/j.jqsrt.2004.05.058

Cox, S. K., & Griffith, K. T. (1979). Estimates of radiative divergence during phase III of the GARP Atlantic tropical experiment: Part II. Analysis of phase III results. *Journal of the Atmospheric Sciences*, *36*(4), 586–601. https://doi.org/10.1175/1520-0469(1979)036<0586:EORDDP>2.0.CO;2

Cronin, T. W., Emanuel, K. A., & Molnar, P. (2015). Island precipitation enhancement and the diurnal cycle in radiative-convective equilibrium. *Quarterly Journal of the Royal Meteorological Society*, *141*(689), 1017–1034. https://doi.org/10.1002/qj.2443

Crueger, T., Giorgetta, M. A., Brokopf, R., Esch, M., Fiedler, S., Hohenegger, C., et al. (2018). ICON-A, The atmosphere component of the ICON Earth system model: II. Model evaluation. *Journal of Advances in Modeling Earth Systems*, *10*(7), 1638–1662. https://doi.org/10.1029/2017MS001233

Dai, A. (2001). Global precipitation and thunderstorm frequencies. Part II: Diurnal variations. *Journal of Climate*, *14*, 1112–1128. https://doi.org/10.1175/1520-0442(2001)014<1112:GPATFP>2.0.CO;2

Dai, A., & Deser, C. (1999). Diurnal and semidiurnal variations in global surface wind and divergence fields. *Journal of Geophysical Research*, *104*(D24), 31109. https://doi.org/10.1029/1999JD900927

Dirmeyer, P. A., Cash, B. A., Kinter, J. L., Jung, T., Marx, L., Satoh, M., et al. (2012). Simulating the diurnal cycle of rainfall in global climate models: Resolution versus parameterization. *Climate Dynamics*, *39*(1-2), 399–418. https://doi.org/10.1007/s00382-011-1127-9

Giorgetta, M. A., Brokopf, R., Crueger, T., Esch, M., Fiedler, S., Helmert, J., et al. (2018). ICON-A, The atmosphere component of the ICON Earth system Model: I. Model description. *Journal of Advances in Modeling Earth Systems*, *10*, 1613–1637. https://doi.org/10.1029/2017MS001242

Gonzalez, A. O., Mora Rojas, G., Schubert, W. H., & Taft, R. K. (2017). Transient aspects of the Hadley circulation forced by an idealized off-equatorial ITCZ. *Journal of Advances in Modeling Earth Systems*, *9*, 668–690. https://doi.org/10.1002/2016MS000837

Gray, W. M., & Jacobson, R. W. (1977). Diurnal variation of deep cumulus convection. *Monthly Weather Review*, *105*, 1171–1188.

Gupta, A. K., Rajeev, K., Sijikumar, S., & Nair, A. K. M. (2018). Enhanced daytime occurrence of clouds in the tropical upper troposphere over land and ocean. *Atmospheric Research*, *201*(February 2017), 133–143. https://doi.org/10.1016/j.atmosres.2017.10.018

Herman, M. J., & Raymond, D. J. (2014). WTG cloud modeling with spectral decomposition of heating. *Journal of Advances in Modeling Earth Systems*, *6*, 1121–1140. https://doi.org/10.1002/2014MS000359

Houze, R. A. (1997). Stratiform precipitation in regions of convection: A meteorological paradox? *Bulletin of the American Meteorological Society*, *78*(10), 2179–2196. https://doi.org/10.1175/1520-0477(1997)078<2179:SPIROC>2.0.CO;2

Iacono, M. J., Delamere, J. S., Mlawer, E. J., Shephard, M. W., Clough, S. A., & Collins, W. D. (2008). Radiative forcing by long-lived greenhouse gases: Calculations with the AER radiative transfer models. *Journal of Geophysical Research*, *113*, D13103. https://doi.org/10.1029/2008JD009944

Jiang, J. H., Su, H., Zhai, C., Janice Shen, T., Wu, T., Zhang, J., et al. (2015). Evaluating the diurnal cycle of upper-tropospheric ice clouds in climate models using SMILES observations. *Journal of the Atmospheric Sciences*, *72*(3), 1022–1044. https://doi.org/10.1175/JAS-D-14-0124.1

Johnson, R. H. (2011). Diurnal cycle of monsoon convection. *The Global Monsoon System: Research and Forecast*, 257–276. Retrieved from https://www.worldscientific.com/worldscibooks/10.1142/8109

Johnson, R. H., Ciesielski, P. E., & Rickenbach, T. M. (2016). A further look at Q1 and Q2 from TOGA COARE. *Meteorological Monographs*, *56*, 1.1–1.12. https://doi.org/10.1175/AMSMONOGRAPHS-D-15-0002.1

Johnson, R. H., Ciesielski, P. E., Ruppert, J. H., & Katsumata, M. (2015). Sounding-based thermodynamic budgets for DYNAMO. *Journal of the Atmospheric Sciences*, *72*(2), 598–622. https://doi.org/10.1175/JAS-D-14-0202.1

Kikuchi, K., & Wang, B. (2008). Diurnal precipitation regimes in the global tropics*. *Journal of Climate*, *21*(11), 2680–2696. https://doi.org/10.1175/2007JCLI2051.1

Klocke, D., Brueck, M., Hohenegger, C., & Stevens, B. (2017). Rediscovery of the doldrums in storm-resolving simulations over the tropical Atlantic. *Nature Geoscience*, *10*(12), 891–896. https://doi.org/10.1038/s41561-017-0005-4

Kraus, E. B. (1963). The diurnal precipitation change over the sea. *Journal of the Atmospheric Sciences*, *20*(6), 551–556. https://doi.org/10.1175/1520-0469(1963)020<0551:TDPCOT>2.0.CO;2

Liu, C., & Moncrieff, M. W. (1998). A numerical study of the diurnal cycle of tropical oceanic convection. *Journal of the Atmospheric Sciences*, *55*(13), 2329–2344. https://doi.org/10.1175/1520-0469(1998)055<2329:ANSOTD>2.0.CO;2

Mapes, B. E., & Houze, R. a. (1993). Cloud clusters and superclusters over the oceanic warm pool. *Monthly Weather Review*, *121*(5), 1398–1416. https://doi.org/10.1175/1520-0493(1993)121<1398:CCASOT>2.0.CO;2

Mapes, B. E., & Houze, R. A. (1995). Diabatic divergence profiles in western Pacific mesoscale convective systems. *Journal of the Atmospheric Sciences*, *52*(10), 1807–1828. https://doi.org/10.1175/1520-0469(1995)052<1807:DDPIWP>2.0.CO;2

Mlawer, E. J., Taubman, S. J., Brown, P. D., Iacono, M. J., & Clough, S. A. (1997). Radiative transfer for inhomogeneous atmospheres: RRTM, a validated correlated-k model for the longwave. *Journal of Geophysical Research*, *102*(D14), 16663. https://doi.org/10.1029/97JD00237

Navarro, E. L., & Hakim, G. J. (2016). Idealized numerical modeling of the diurnal cycle of tropical cyclones. *Journal of the Atmospheric Sciences*, *73*(10), 4189–4201. https://doi.org/10.1175/JAS-D-15-0349.1

Nesbitt, S. W., & Zipser, E. J. (2003). The diurnal cycle of rainfall and convective intensity according to three years of TRMM measurements. *Journal of Climate*, *16*(10), 1456–1475. https://doi.org/10.1175/1520-0442-16.10.1456

Nicholls, M. E. (2015). An investigation of how radiation may cause accelerated rates of tropical cyclogenesis and diurnal cycles of convective activity. *Atmospheric Chemistry and Physics Discussions*, *15*(5), 6125–6205. https://doi.org/10.5194/acpd-15-6125-2015

Nitta, T., & Esbensen, S. (1974). Diurnal variations in the western Atlantic trades during the BOMEX. *Journal of the Meteorological Society of Japan*, *52*(2), 254–257.

O'Neill, M. E., Perez-Betancourt, D., & Wing, A. A. (2017). Accessible environments for diurnal-period waves in simulated tropical cyclones. *Journal of the Atmospheric Sciences*, *74*(8), 2489–2502. https://doi.org/10.1175/JAS-D-16-0294.1

Powell, S. W., Houze, R. A., Kumar, A., & McFarlane, S. A. (2012). Comparison of simulated and observed continental tropical anvil clouds and their radiative heating profiles. *Journal of the Atmospheric Sciences*, *69*(9), 2662–2681. https://doi.org/10.1175/JAS-D-11-0251.1

Randall, D. A., Harshvardhan, & Dazlich, D. A. (1991). Diurnal variability of the hydrologic cycle in a general circulation model. *Journal of the Atmospheric Sciences*, *48*(1), 40–62. https://doi.org/10.1175/1520-0469(1991)048<0040:DVOTHC>2.0.CO;2

Ruppert, J. H. (2016). Diurnal timescale feedbacks in the tropical cumulus regime. *Journal of Advances in Modeling Earth Systems*, *8*, 1483–1500. https://doi.org/10.1002/2016MS000713

Ruppert, J. H., & Hohenegger, C. (2018). Diurnal circulation adjustment and organized deep convection. *Journal of Climate*, *31*(12), 4899–4916. https://doi.org/10.1175/JCLI-D-17-0693.1

Ruppert, J. H., & Johnson, R. H. (2015). Diurnally modulated cumulus moistening in the preonset stage of the Madden-Julian Oscillation during DYNAMO*. *Journal of the Atmospheric Sciences*, *72*(4), 1622–1647. https://doi.org/10.1175/JAS-D-14-0218.1

Ruppert, J. H., & Johnson, R. H. (2016). On the cumulus diurnal cycle over the tropical warm pool. *Journal of Advances in Modeling Earth Systems*, *8*, 669–690. https://doi.org/10.1002/2015MS000610

Ruppert, J. H., & O'Neill, M. E. (2019). Diurnal cloud and circulation changes in simulated tropical cyclones. *Geophysical Research Letters*, *46*, 502–511. https://doi.org/10.1029/2018GL081302

Schulz, H., & Stevens, B. (2018). Observing the tropical atmosphere in moisture space. *Journal of the Atmospheric Sciences*, *75*(10), 3313–3330. https://doi.org/10.1175/JAS-D-17-0375.1

Schumacher, C., Zhang, M. H., & Ciesielski, P. E. (2007). Heating structures of the TRMM field campaigns. *Journal of the Atmospheric Sciences*, *64*(7), 2593–2610. https://doi.org/10.1175/JAS3938.1

Sobel, A. H., Nilsson, J., & Polvani, L. M. (2001). The weak temperature gradient approximation and balanced tropical moisture waves*. *Journal of the Atmospheric Sciences*, *58*(23), 3650–3665. https://doi.org/10.1175/1520-0469(2001)058<3650:TWTGAA>2.0.CO;2

Soden, B. J. (2000). The diurnal cycle of convection, clouds, and water vapor in the tropical upper troposphere. *Geophysical Research Letters*, *27*(15), 2173–2176. https://doi.org/10.1029/2000GL011436

Sui, C.-H., Lau, K.-M., Takayabu, Y. N., & Short, D. A. (1997). Diurnal variations in tropical oceanic cumulus convection during TOGA COARE. *Journal of the Atmospheric Sciences*, *54*(1990), 639–655.

Webster, P. J., Clayson, C. A., & Curry, J. A. (1996). Clouds, radiation, and the diurnal cycle of sea surface temperature in the tropical western Pacific. *Journal of Climate*, *9*(8), 1712–1730. https://doi.org/10.1175/1520-0442(1996)009<1712:CRATDC>2.0.CO;2

Webster, P. J., & Stephens, G. L. (1980). Tropical upper-tropospheric extended clouds: Inferences from winter MONEX. *Journal of the Atmospheric Sciences*, *37*(7), 1521–1541. https://doi.org/10.1175/1520-0469-37.7.1521

Wheeler, M., & Kiladis, G. N. (1999). Convectively coupled equatorial waves: Analysis of clouds and temperature in the wavenumber-frequency domain. *Journal of the Atmospheric Sciences*, *56*(3), 374–399. https://doi.org/10.1175/1520-0469(1999)056<0374:CCEWAO>2.0.CO;2

Wood, R., Bretherton, C. S., & Hartmann, D. L. (2002). Diurnal cycle of liquid water path over the subtropical and tropical oceans. *Geophysical Research Letters*, *29*(23), 2092. https://doi.org/10.1029/2002GL015371

Wu, Q., & Ruan, Z. (2016). Diurnal variations of the areas and temperatures in tropical cyclone clouds. *Quarterly Journal of the Royal Meteorological Society*, *142*(700), 2788–2796. https://doi.org/10.1002/qj.2868

Yang, S., & Smith, E. A. (2006). Mechanisms for diurnal variability of global tropical rainfall observed from TRMM. *Journal of Climate*, *19*(20), 5190–5226. https://doi.org/10.1175/JCLI3883.1

Zängl, G., Reinert, D., Rípodas, P., & Baldauf, M. (2015). The ICON (ICOsahedral Non-hydrostatic) modelling framework of DWD and MPI-M: Description of the non-hydrostatic dynamical core. *Quarterly Journal of the Royal Meteorological Society*, *141*(687), 563–579. https://doi.org/10.1002/qj.2378

Zipser, E. J. (1977). Mesoscale and convective-scale downdrafts as distinct components of squall-line structure. *Monthly Weather Review*, *105*, 1568–1589.